Nuclear Materials and Energy 18 (2019) 321–325

Contents lists available at ScienceDirect

Nuclear Materials and Energy

journal homepage: www.elsevier.com/locate/nme

Influence of thermal shocks on the He induced surface morphology on tungsten

Y. Hamaji[a,*], M. Tokitani[a], A. Kreter[b], R. Sakamoto[a], A. Sagara[a,c], H. Tamura[a], S. Masuzaki[a]

[a] National Institutes of Natural Sciences, National Institute for Fusion Science, 322-6 oroshi-cho, Toki 509-5292, Japan
[b] Forschungszentrum Jülich GmbH, Institut für Energie- und Klimaforschung - Plasmaphysik, 52425 Jülich, Germany
[c] SOKENDAI, SOKENDAI (The Graduate University for Advanced Studies), 322-6 Oroshi, Toki, Gifu 509-5292, Japan

ARTICLE INFO

Keywords:
Tungsten
Divertor
He induced surface morphology
Thermal shocks

ABSTRACT

In this study, the effect of ELM-like thermal shocks on He induced surface morphology were investigated. A W sample was exposed to pure He plasma. He ion incident energy, flux and fluence were 80 eV, 1×10^{22} /m^2/s and 3×10^{25} /m^2, respectively. Irradiation temperature were approximately 470 and 1100 K. Then, thermal shocks were applied on the sample using focused electron beam. The peak heat flux, pulse duration and base temperature were 500 MW/m^2, 500 μs and R.T., respectively. After the thermal shocks, He induced morphologies such as holes and periodic undulations were flatten completely at the region exposed to the highest heat flux. At the peripheral regions of the electron beam spot, the hole density increase or partial flattening of morphologies were observed. These results suggested that in order to anticipate surface morphology with He irradiation and ELMs, the peak temperature should play a more important role than base temperature.

1. Introduction

Tungsten (W) has good properties to be a plasma facing material (PFM), such as high thermal conductivity, low Tritium retention and low sputtering yield. W is a promising candidate for plasma facing components in future reactors such as ITER and beyond. Plasma facing materials are bombarded by Helium (He) ash as well as by hydrogen isotopes. In addition, W materials in Tokamak will suffer from thermal shocks caused by Edge Localized Mode (ELM).

He implantation induces modification of surface morphologies [1–7] and hydrogen isotopes behavior [8–10]. Therefore, the He behavior on W surface is an important subject. It is known that the temperature have huge impact on the He induced morphologies such as He bubbles, holes, undulations and fiber-like nano-structure. After the first report of formation of fiber-like nano-structure (also known as “fuzz”) in ref. [2], the formation conditions have been studied in detail. In ref. [5], it is reported that He irradiation in the temperature range between 1000 K and 2000 K cause formation of fiber-like nano-structure in various devices. Detailed observation using SEM (Scanning Electron Microscope) and TEM (Transmission Electron Microscope) revealed the existence of more fine He induced surface morphology such as He bubbles and surface undulation even in the irradiation temperature below 1000 K [3]. In order to understand the influence of ELM-like thermal shocks on these He induced surface structures, several experimental studies were conducted [11–17]. For instance, on fiber-like nano-structure severe modification of He induced fiber-like nano-structure were observed in samples exposed thermal shocks after He plasma exposure as well as simultaneous exposure to He plasma and thermal shocks (see ref. [12]). These results suggest that the timescale of ELM-like thermal shocks (typically upto 1 ms) is enough long to modify the He induced structure. These effects might correlate with the rapid temperature rise followed by decline by thermal shocks. The fast heating/cooling induces thermal stress, increase of He bubbles's internal pressure, migration and coalescence of He bubbles and enhancement of surface migration of W atoms. The thermal stress is recognized as the cause of crack formation by thermal shocks [18]. However, the effect of thermal shocks on the fine surface structures like undulations reported in ref. [3] have not been reported.

In this study, we focused on the effect of thermal shocks on He induced surface morphologies such as He bubbles, holes and undulations. The change of He induced surface morphology on W samples by following exposure to ELM-like thermal shocks were observed by SEM (Scanning electron Microscope) and TEM (Transmission electron Microscope).

2. Experimental

The samples were high-purity (99.995 > %) W manufactured by Toho Kinzoku Co. Ltd. with a square shape of 20 × 20 mm and 5 mm

* Corresponding author.
E-mail address: hamaji.yukinori@nifs.ac.jp (Y. Hamaji).

https://doi.org/10.1016/j.nme.2019.01.029
Received 13 August 2018; Received in revised form 30 January 2019; Accepted 30 January 2019
Available online 01 February 2019

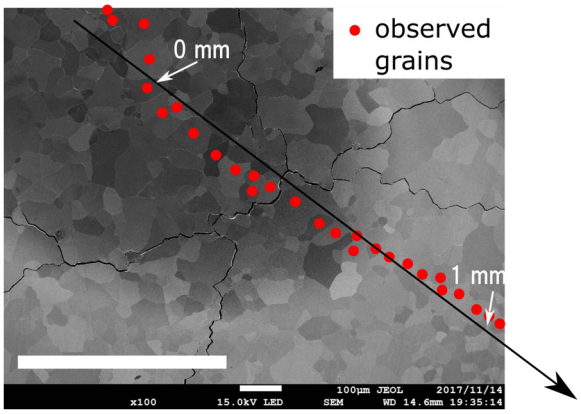

Fig. 1. SEM image of a sample after thermal shocks. This sample was exposed to He plasma at 1100 K. axis red points indicates observed grains for Fig. 5.

thickness. The surface was mechanically polished and then annealed at 1773 K for 2 h in vacuum. He plasma exposures were performed using linear plasma device PSI-2 at Forschungszentrum Jülich [19]. Irradiation temperatures were approximately 470 and 1100 K. The typical He flux and fluence were 1×10^{22} /m^2/s and 3×10^{25} /m^2, respectively. The samples were biased - 100 V during exposures. The typical incident energy of He ion was 78 eV. After the He irradiation, thermal shocks were applied on the samples in high heat flux test facility with electron beam facility Active Cooling Teststand 2 (ACT2) [20]. The electron beam had Gaussian-like profile with the FWHM of approximately 6.5 mm. The peak heat flux, cycle numbers, base temperature and the duration of the thermal shocks were about 500 MW/m^2, 10 cycles, room temperature (300 K) and 500 μs, respectively. Beam was transferred between the beam dump and the sample by electromagnetic deflection lenses at translation speeds greater than 500 m/s. During thermal shock, no beam rastering was performed. Therefore, heat flux distribution was the same as the e-beam profile. The detailed center of irradiation spot of each sample were determined by eye based on the crack distribution after the experiment. In this paper, surface morphology changes at each distance from the center of e-beam spot will be discussed below. It should be noted that the distance has significant error due to the error of the center of e-beam irradiation spot. Fig. 1 shows an SEM image of a sample exposed to He plasma at 1100 K. Center of beam spot is indicated as “0 mm” and observed grains are shows in red points.

Surface morphology was observed using SEM and TEM. Samples were not tilted during SEM observations. In TEM observations, small thin pieces were cut out from the sample surface using Focused Ion Beam (FIB) system. In order to observe the surface clearly and to protect the surface from the FIB's ion beam, carbon (C) layer was deposited by depositing feature of the FIB device. Holes formed by He irradiation were characterized using image processing software ImageJ [21]. Holes were detected by ImageJ with the parameters of circularity and minimum hole size were 0.25–1.00 and 30 nm^2, respectively. The circularity of 1 indicates perfect circle. All SEM images for image processing were in the same magnification shown in Fig. 2.

3. Results and discussion

3.1. Typical surface morphology by He irradiation

Fig. 2 shows the typical surface morphologies formed by He irradiation at low (470 K) and high (1100 K) temperature. These images were taken before the thermal shocks. Both of the irradiation temperature were below threshold of formation of fiber-like nano-structure. Undulations ((a) and (d)) and jagged edges ((b) and (e)) were observed. In addition, some grains show no undulation or jagged edges ((c) and (f)). Different grains showed different characteristics of surface morphologies. A strong correlation between these differences of morphology and the grain orientation have been reported [4]. No obvious temperature dependence of surface morphology were observed except holes observed in samples irradiated at high temperature. Typical size of holes were from several nm upto 30 nm in diameter. These holes should be caused by He bubbles that reached the surface during He irradiation.

From TEM observation, there were indications of temperature dependence of properties of He bubbles. Fig. 3 shows typical TEM images of samples irradiated at 470 K (a) and at 1100 K (b). In Fig. 3(a), dense small bubbles with diameter around 1 nm (indicated with white arrows) and few larger bubbles with diameter about 5 nm (indicated by white dashed circle) were observed. He bubbles distributed below 15 nm in depth. On the other hand, larger bubbles and deeper distribution of bubbles were observed in samples irradiated at 1100 K (Fig. 3(b)). These results should be caused by higher rate of migration of He bubbles and coalescence of multiple bubbles. They are consistent with some previous studies [4,22–24]. Holes indicated by black arrows should

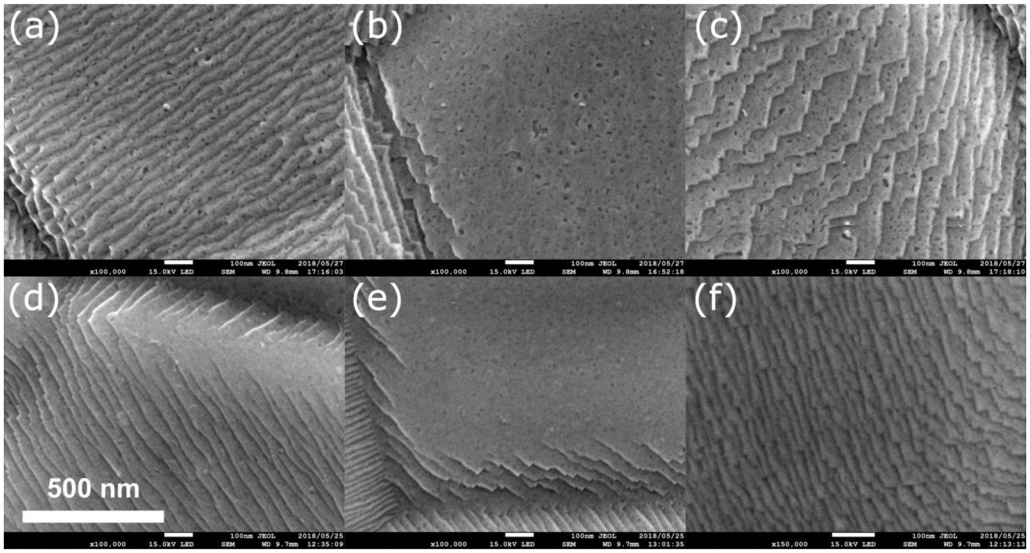

Fig. 2. SEM images of typical surface morphologies observed in the samples irradiated by He. (a), (b) and (c): taken from a sample irradiated at 470 K. (d), (e) and (f): taken from a sample irradiated at 1100 K.

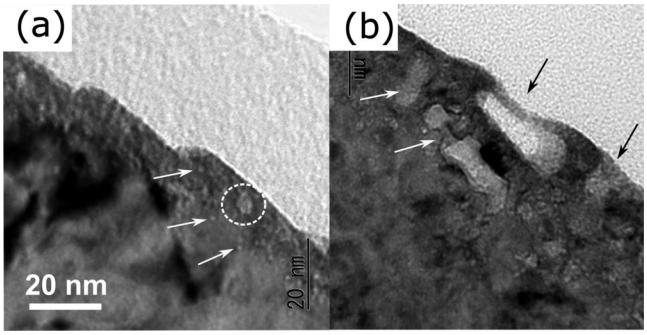

Fig. 3. Cross-sectional images observed by TEM of samples irradiated by He at (a) 470 K and (b) 1100 K.

formed by large bubbles what reached the surface. The non-circular bubbles below the surface indicated by white arrows in Fig. 3(b) suggest that bubble's coalescence have significant impact for growth of He bubbles.

3.2. Surface morphology change by thermal shocks

SEM images observed after thermal shocks were shown in Fig. 4. Fig. 4(a) is a typical image of a grain around the center of e-beam spot of samples irradiated at low temperature. The surface morphologies such as undulations and holes were completely flatten. In the peripheral regions of e-beam spot (~ 0.5 mm from the center), partial flattening such as in Fig. 4(b) was observed. In the case of samples that experienced He irradiation at high temperature, the similar flattened surface was observed at the center of e-beam spot (see Fig. 4(c)). Fig. 4(d) shows partially flattened surface in the peripheral region of e-beam spot (~ 0.6 mm from the center) in a sample irradiated by He at high temperature. These flattenings suggest that significant surface migration of W atoms occurred by temperature rise during thermal shocks. The difference of the peak temperature should induce the different degree of flattening. The surface shows large holes with more than 10 nm in diameter with relatively less density. Dense holes found in the sample before the thermal shocks with several nm in diameter

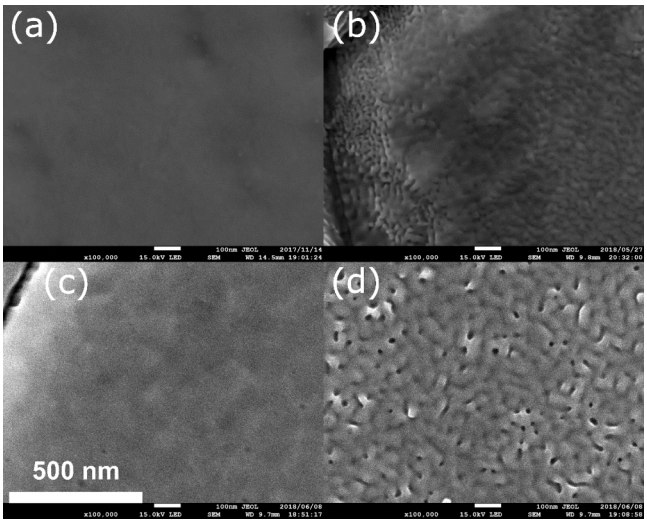

Fig. 4. SEM images of samples after the thermal shock experiments. (a): at the center of e-beam spot on the sample which experienced the He irradiation at 470 K. (b): at the about location what is 0.5 mm distant from the center of e-beam spot on the sample which experienced the He irradiation at 470 K. (c): at the center of e-beam spot on the sample which experienced the He irradiation at 1100 K. (d): at the about location what is 0.5 mm distant from the center of e-beam spot on the sample which experienced the He irradiation at 1100 K.

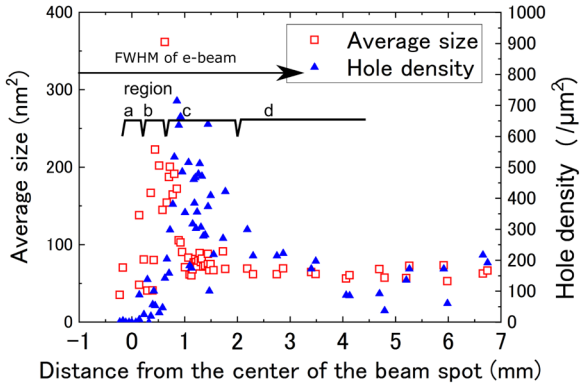

Fig. 5. Hole density and average size of holes plotted against distance from the center of the e-beam spot of the sample experienced He irradiation at 1100 K.

disappeared. In this region, flattening driven by W atom's surface migration should be less than that at the center of e-beam spot. Therefore, large holes could survive.

The hole density and average size of holes are plotted against the distance from the center of e-beam spot in Fig. 5. The characteristics of hole distribution can be separated into four regions according to the distance. Region a is from 0 to 0.2 mm. In this region, holes and the surface morphology were completely flattened and very few holes were detected. Fig. 4(c) is categorized in this region. From 0.2 to 0.6 mm is region b. Typical image of this region is Fig. 4(d). As described in the previous paragraph, the average size of holes was larger than that of region d. Region c is from 0.6 to 2.0 mm. The hole density is larger than that at outside of the spot and average size were roughly the same to the outside. Fig. 6 is a comparison between SEM images taken before (a) and after (b) the thermal shocks at the same location. The number of holes in the image of after the thermal shock experiment is apparently larger than before. The close-up images in Fig. 6 show the same hole indicated by arrows that survived the thermal shock surrounded by holes newly generated by thermal shocks. In the region d (more than 2.0 mm), the hole density and the average size are roughly the same as that at outside the spot.

Cross-sectional observation was carried out by TEM. Fig. 7(a) and (b) are the TEM images taken from a sample experienced He irradiation at high temperature before and after the thermal shock experiments, respectively. Fig. 7(b) was taken from the region b. There is a layer without bubbles with about 20 nm in the thickness in Fig. 7(b) unlike there being bubbles in the depth before thermal shock experiment (see Fig. 7(a)). This layer is consistent with flattened and less dense holes observed in SEM observation. However, there are survived He bubbles in deeper region (more than 20 nm) in Fig. 7(b). In addition, these bubbles appear to be relatively spherical compared with bubbles shown in Fig. 7(a).

The mechanism of surface morphology change is still unclear. However, annealing effect should play important role for these results.

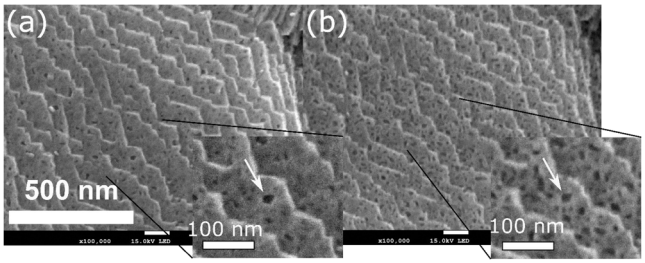

Fig. 6. Comparison between SEM images before (a) and after (b) the thermal shock experiment taken at the same position of a sample experienced He irradiation at 1100 K. This location belongs to the region b in the Fig. 5.

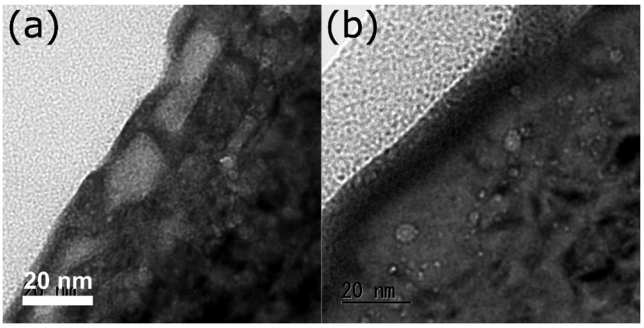

Fig. 7. Cross-sectional TEM images taken from a sample experienced He irradiation at 1100 K. (a): before the thermal shock experiment. (b): after the thermal shock experiment.

Kinetic effect of incident electron should be a less important factor because the incident energy is only 40 keV. As reported in previous studies [11–15], He induced fiber-like nano-structure can be modified in this timescale. The possible factors that should take place during thermal shocks are He bubble's migration, W atom's migration, pressure increase of He bubbles, reduction of deformation threshold of W lattice and induced thermal stress. These phenomena are activated by higher temperature. The pressure increase of He bubbles, He bubble migration and reduction of deformation threshold of lattice might induce bursting He bubbles at the surface. These bursted bubbles (holes) should be flattened by W atom's migration. The difference between completely flattened surface and surface with higher density of holes might be due to the difference of contribution of W atom's migration. Due to the error of heat flux distribution and estimated location of center of the beam spot, it is impossible to estimate heat flux on each regions accurately. However, with assumption of Gaussian heat flux distribution with 500 MW/m^2 peak heat flux and 6.5 mm FWHM, applied heat flux of region a, b, c and d were estimated 500–499, 499–490, 490–393 and lower than 394 MW/m^2 respectively. In order to make a rough estimate of maximum temperature at each regions, one dimensional thermal diffusion with constant thermal properties were assumed (thermal conductivity, heat capacity and density are 164 J/m/K, 130 J/kg and 19,300 kg/m^3, respectively). The estimated maximum temperatures of region a, b, c and d are 922–921, 921–909, 909–789 and less than 789 K respectively. The observed modification of surface morphology occurred in the regions applied more than 80% of the peak heat flux. Observed morphology changes were limited very narrow area. A previous research reported that threshold temperature of hole formation between 773 and 1073 K [4]. That suggest the mechanism of morphology changes have a threshold less than 1000 K. In addition, there might be unrevealed changes in the region exposed to lower than 390 MW/m^2. Further detailed observation is required to understand these phenomena.

4. Summary

In this study, the effect of ELM-like thermal shocks on He induced surface morphology was investigated. He induced surface morphology was formed below threshold temperature of forming fiber-like nano-structure (about 470 K and 1100 K). By SEM observation, He induced morphologies such as periodic undulation and jagged edges were found in the samples with low and high temperature He irradiation. Dense holes were observed in samples experienced He irradiation at high temperature. After the He ion irradiation, ELM-like thermal shocks were applied by high heat flux test facility using electron beam. The thermal shocks significantly deformed the surface morphology. The deformation was consistent with the heat flux distribution due to profile of the e-beam. In the regions with highest heat flux, the surface morphology was completely flatten. The partial flattening and hole density increase were observed at the regions exposed to relatively lower heat flux. TEM observation revealed disappearing of the He bubbles at near surface (~20 nm in depth) and existence of survived bubbles in deeper region. The mechanism of surface morphology change is still unclear. However, temperature rise during the thermal shocks should play important role for the results. During annealing process, He and the bubble migration, W atom's surface migration and reduction of deformation threshold of lattice are supposed to be take place. In addition the pressure increase of He bubbles, He bubble migration and reduction of deformation threshold of lattice might induce bursting He bubbles at the surface. The bursted bubbles (holes) should be flatten by W atom's migration. The difference between completely flatten surface and surface with higher density of holes might be due to the difference of contribution of W atom's migration.

One of the findings of this work is that the duration of ELM-like thermal shock (500 μs) is long enough to change not only fiber-like nano-structure but also on undulations or holes induced in lower He irradiation temperature. However, due to poor accuracy of local heat flux and absence of peak temperature, quantitative correlation between heat flux and morphology changes are not clear. In order to achieve detailed understanding of this, further experiments and numerical modeling are required. Especially, the effect of local temperature during thermal shock, duration of the thermal shock and the base temperature are important to confirm the influence of temperature.

Acknowledgments

The authors gratefully acknowledge the staff of the PSI-2 team for their experimental support and Mr. D. Nagata for TEM observations. This work was supported by NIFS research budget (code ULFF032) and International Energy Agency Technology Collaboration Programme on the Development and Research on Plasma Wall Interaction Facilities for Fusion Reactors (IEA PWI TCP).

References

[1] M.J. Baldwin, R.P. Doerner, Helium induced nanoscopic morphology on tungsten under fusion relevant plasma conditions, Nucl. Fusion 48 (2008) 035001, , https://doi.org/10.1088/0029-5515/48/3/035001.
[2] S. Takamura, N. Ohno, D. Nishijima, S. Kajita, Formation of nanostructured tungsten with arborescent shape due to helium plasma irradiation, Plasma Fusion Res. 1 (2006), https://doi.org/10.1585/pfr.1.051 051–051.
[3] M. Miyamoto, S. Mikami, H. Nagashima, N. Iijima, D. Nishijima, R.P. Doerner, N. Yoshida, H. Watanabe, Y. Ueda, A. Sagara, Systematic investigation of the formation behavior of helium bubbles in tungsten, J. Nucl. Mater. 463 (2015) 333–336, https://doi.org/10.1016/j.jnucmat.2014.10.098.
[4] R. Sakamoto, E. Bernard, A. Kreter, N. Yoshida, Surface morphology of tungsten exposed to helium plasma at temperatures below fuzz formation threshold 1073K, Nucl. Fusion 57 (2017) 016040, , https://doi.org/10.1088/1741-4326/57/1/016040.
[5] S. Kajita, W. Sakaguchi, N. Ohno, N. Yoshida, T. Saeki, Formation process of tungsten nanostructure by the exposure to helium plasma under fusion relevant plasma conditions, Nucl. Fusion 49 (2009) 095005, , https://doi.org/10.1088/0029-5515/49/9/095005.
[6] G. De Temmerman, T. Hirai, R.A. Pitts, The influence of plasma-surface interaction on the performance of tungsten at the ITER divertor vertical targets, Plasma Phys. Control. Fusion (2018) 60, https://doi.org/10.1088/1361-6587/aaaf62.
[7] R.P. Doerner, D.L. Rudakov, C.P. Chrobak, A.R. Briesemeister, C. Corr, G. De Temmerman, P. Kluth, C.J. Lasnier, A.G. McLean, D.C. Pace, R.A. Pitts, O. Schmitz, M. Thompson, V. Winters, Investigation of He-W interactions using DiMES on DIII-D, Phys. Scr. (2016), https://doi.org/10.1088/0031-8949/T167/1/014054 2016.
[8] O.V. Ogorodnikova, T. Schwarz-Selinger, K. Sugiyama, V.K. Alimov, Deuterium retention in tungsten exposed to low-energy pure and helium-seeded deuterium plasmas, J. Appl. Phys. 109 (2011) 013309, , https://doi.org/10.1063/1.3505754.
[9] H.T. Lee, H. Tanaka, Y. Ohtsuka, Y. Ueda, Ion-driven permeation of deuterium through tungsten under simultaneous helium and deuterium irradiation, J. Nucl. Mater. 415 (2011) S696–S700, https://doi.org/10.1016/j.jnucmat.2010.12.023.
[10] V.K. Alimov, B. Tyburska-Püschel, Y. Hatano, J. Roth, K. Isobe, M. Matsuyama, T. Yamanishi, The effect of displacement damage on deuterium retention in ITER-grade tungsten exposed to low-energy, high-flux pure and helium-seeded deuterium plasmas, J. Nucl. Mater. 420 (2012) 370–373, https://doi.org/10.1016/j.jnucmat.2011.10.025.
[11] N. Lemahieu, H. Greuner, J. Linke, H. Maier, G. Pintsuk, M. Wirtz, G. Van Oost, J.M. Noterdaeme, Thermal shock behaviour of H and H/He-exposed tungsten at high temperature, Phys. Scr. (2016), https://doi.org/10.1088/0031-8949/T167/1/

014008 2016.
[12] M. Wirtz, M. Berger, A. Huber, A. Kreter, J. Linke, G. Pintsuk, M. Rasinski, G. Sergienko, B. Unterberg, Influence of helium induced nanostructures on the thermal shock performance of tungsten, Nucl. Mater. Energy 9 (2016) 177–180, https://doi.org/10.1016/j.nme.2016.07.002.
[13] L. Buzi, G. De Temmerman, A.E. Huisman, S. Bardin, T.W. Morgan, M. Rasinski, R.A. Pitts, G. Van Oost, Response of tungsten surfaces to helium and hydrogen plasma exposure under ITER relevant steady state and repetitive transient conditions, Nucl. Fusion (2017) 57, https://doi.org/10.1088/1741-4326/aa81e4.
[14] M. Wirtz, A. Kreter, J. Linke, T. Loewenhoff, G. Pintsuk, G. Sergienko, I. Steudel, B. Unterberg, E. Wessel, High pulse number thermal shock tests on tungsten with steady state particle background, Phys. Scr. T170 (2017) 014066, , https://doi.org/10.1088/1402-4896/aa909e.
[15] G. De Temmerman, T.W. Morgan, G.G. van Eden, T. de Kruif, M. Wirtz, J. Matejicek, T. Chraska, R.A. Pitts, G.M. Wright, Effect of high-flux H/He plasma exposure on tungsten damage due to transient heat loads, J. Nucl. Mater. 463 (2015) 198–201, https://doi.org/10.1016/j.jnucmat.2014.09.075.
[16] G. De Temmerman, J.J. Zielinski, S. van Diepen, L. Marot, M. Price, ELM simulation experiments on Pilot-PSI using simultaneous high flux plasma and transient heat/particle source, Nucl. Fusion 51 (2011) 073008, , https://doi.org/10.1088/0029-5515/51/7/073008.
[17] G. De Temmerman, K. Bystrov, R.P. Doerner, L. Marot, G.M. Wright, K.B. Woller, D.G. Whyte, J.J. Zielinski, Helium effects on tungsten under fusion-relevant plasma loading conditions, J. Nucl. Mater. 438 (2013) S78–S83, https://doi.org/10.1016/j.jnucmat.2013.01.012.
[18] C. Li, D. Zhu, X. Li, B. Wang, J. Chen, Thermal–stress analysis on the crack formation of tungsten during fusion relevant transient heat loads, Nucl. Mater. Energy 13 (2017) 68–73, https://doi.org/10.1016/j.nme.2017.06.008.
[19] A. Kreter, C. Brandt, A. Huber, S. Kraus, S. Moeller, M. Reinhart, B. Schweer, G. Sergienko, B. Unterberg, Linear plasma device PSI-2 for plasma-material interaction studies, Fusion Sci. Technol. 68 (2015) 8–14, https://doi.org/10.13182/FST14-906.
[20] Y. Hamaji, M. Tokitani, S. Masuzaki, R. Sakamoto, H. Tamura, A. Sagara, ACT2: a high heat flux test facility using electron beam for fusion, Plasma Fusion Res. 11 (2016) 1–4, https://doi.org/10.1585/pfr.11.2405089 2405089.
[21] C.A. Schneider, W.S. Rasband, K.W. Eliceiri, NIH Image to ImageJ: 25 years of image analysis, Nat. Methods 9 (2012) 671 http://dx.doi.org/10.1038/nmeth.2089.
[22] M. Miyamoto, T. Watanabe, H. Nagashima, D. Nishijima, R.P. Doerner, S.I. Krasheninnikov, A. Sagara, N. Yoshida, *In situ* transmission electron microscope observation of the formation of fuzzy structures on tungsten, Phys. Scr. T159 (2014) 014028, , https://doi.org/10.1088/0031-8949/2014/T159/014028.
[23] M. Miyamoto, S. Mikami, H. Nagashima, N. Iijima, D. Nishijima, R.P. Doerner, N. Yoshida, H. Watanabe, Y. Ueda, A. Sagara, Systematic investigation of the formation behavior of helium bubbles in tungsten, J. Nucl. Mater. 463 (2015) 333–336, https://doi.org/10.1016/j.jnucmat.2014.10.098.
[24] G.M. Wright, D. Brunner, M.J. Baldwin, K. Bystrov, R.P. Doerner, B. Labombard, B. Lipschultz, G. De Temmerman, J.L. Terry, D.G. Whyte, K.B. Woller, Comparison of tungsten nano-tendrils grown in Alcator C-Mod and linear plasma devices, J. Nucl. Mater. 438 (2013) S84–S89, https://doi.org/10.1016/j.jnucmat.2013.01.013.